Cold Regions Science and Technology 65 (2011) 372–381

Contents lists available at ScienceDirect

Cold Regions Science and Technology

journal homepage: www.elsevier.com/locate/coldregions

Anticrack model for skier triggering of slab avalanches

J. Heierli [a,b,*], K.W. Birkeland [c], R. Simenhois [d], P. Gumbsch [a,b]

[a] Karlsruhe Institute of Technology, IZBS Institute for Reliability of Components and Systems, Kaiserstr. 12, 76131 Karlsruhe, Germany
[b] Fraunhofer-Institut für Werkstoffmechanik IWM, Wöhlerstr. 11, 79108 Freiburg, Germany
[c] USDA Forest Service National Avalanche Center, Bozeman, MT 59771, USA
[d] Coeur Alaska, Juneau, AK 99803, USA

ARTICLE INFO

Article history:
Received 24 June 2010
Accepted 14 October 2010

Keywords:
Anticrack
Fracture
Slab avalanche
Skier triggering
Snow

ABSTRACT

Skiers caught in a slab avalanche often trigger the avalanche themselves. Preventing those accidents necessitates a better understanding of the factors contributing to the failure of the snowpack under the action of a skier. In the present work, a mathematical model based on the principles of mixed-mode anticracking is proposed for skier triggering. The respective influences of the slope-normal and slope-parallel components of the load exerted by a skier on the prospective fracture plane are taken into account. A criterion for fracture propagation under typical skier loads is derived. It manifests a small number of factors that, combined, multiply the risk of triggering an avalanche. The criterion indicates, contrary to a common perception, that fracture is not more difficult to trigger in gentle slopes than in steep slopes. This major result of the model is confirmed by data obtained from field experiments.

1. Introduction

Each year, snow avalanches cause hundreds and occasionally thousands of fatalities worldwide. In both Europe and North America, professional and recreational skiers represent a large proportion of avalanche fatalities over the past decades. In about 9 out of 10 accidents, the avalanche victims or members of their party trigger the avalanche in which they are caught (e.g., McCammon and Haegeli, 2006). Thus, understanding what conditions favor skier triggering is important for both educational purposes and avalanche forecasting.

Slab avalanches develop when a weak subsurface layer fractures over a large area. The fracture process can occur with or without shear loading and for arbitrary amounts of crack face friction (Heierli et al., 2008; Heierli and Zaiser, 2008). During the fracture process, the snowpack layers above the fracture plane are quickly debonded from the layers below. If the slope is steep enough, the frictional contact forces in the freshly formed fracture plane are insufficient to balance the gravitational pull and the snow begins to slide (van Herwijnen and Heierli, 2009). The prospective fracture plane is in general identified with weak subsurface layers including both persistent and non-persistent forms (see Jamieson, 1995, p. 10). Persistent weak layers consist of surface hoar, depth hoar, and faceted crystals and can be triggered for weeks or months. Non-persistent weak layers consist of new and decomposing snow crystals. These layers typically stabilize within hours or days.

For many years, the approach to skier triggering of snow slab avalanches has been based on the principle that the snowpack fails if the shear stress exerted by slab and skier on the prospective fracture plane exceeds the shear strength of the material in this plane (Föhn, 1987, "stability index"). Since the shear stress increases with increasing slope angle while the strength remains a constant or decreases, this assumption implies that fracture should be easier to initiate on steeper slopes. The approach suffers two conceptual problems: first, by assuming a reproducible stress limit, local stress concentrations near flaws and heterogeneities in the material are discarded (e.g., Lawn, 1993). Second, the fact that weak snowpack layers most often collapse during fracture is not taken into account. The decrease in volume enables failure by anticrack propagation (Heierli et al., 2008). Anticracks, as opposed to simple shear cracks, allow for mechanical work to be done by the compressive component of the load since the collapse provides a small but sufficient room for slope-normal displacements in the crack region. (In simple shear mode, since the displacements are in slope-parallel direction, the compressive loads are perpendicular to the displacements and no mechanical work results.) Experimental evidence has shown that the particular fracture mode of anticracking is likely the rule for the failure of persistent weak subsurface layers and that it also takes place in non-persistent weak layers (van Herwijnen and Jamieson, 2005; van Herwijnen et al., 2010).

Field experiments on skier triggering are not abundant. van Herwijnen and Jamieson (2005) measured the deformation and deformation rate of the snowpack under skier loading and observed crack propagation within the weak layer on two occasions. Schweizer et al. (1995) and Schweizer and Camponovo (2001) measured the normal stress applied by a skier on a horizontal snowpack. These

* Corresponding author. Karlsruhe Institute of Technology, IZBS Institute for Reliability of Components and Systems, Kaiserstr. 12, 76131 Karlsruhe, Germany.
E-mail address: joachim.heierli@kit.edu (J. Heierli).

0165-232X/$ – see front matter © 2010 Elsevier B.V. All rights reserved.
doi:10.1016/j.coldregions.2010.10.008

studies are mainly descriptive and provide no physical framework aimed at the understanding of the fracture process. Numerical simulations presenting insights into the process of skier triggering have recently been carried out by Mahajan et al. (2010). The simulations indicate that collapse propagation by anticracking of the weak layer is the predominant mechanism for fracture initiation unless the fracture energy for mode II is about an order of magnitude smaller than that for the anticrack mode.

In the present article, we develop a detailed mathematical model of skier triggering based on the principles of mixed-mode anticracking (Fletcher and Pollard, 1981). The slope-normal and slope-parallel components of the stress field exerted by a skier in the prospective fracture plane and the depth to which the skis penetrate into the snowpack are taken into account. The calculation is based on the superposition principle for linear materials and leads to a criterion for fracture initiation in dry weak layers by a skier. We especially investigate the influence of the slope angle on the triggering of fracture in persistent weak layers and validate the theoretical results with field experiments. Conceptually, the present calculation resolves a singularity in the stress field, which was contained in an earlier model of skier triggering by collapse of the weak layer (Heierli and Zaiser, 2008, Appendix B).

2. Mathematical model

The two-dimensional situation shown in Fig. 1 is considered. On a slope of angle θ with the horizontal, a homogeneous slab of uniform thickness h and bulk density ϱ rests on a weakly aggregated, cohesive-granular subsurface layer. The cohesion between the grains composing the weak layer prevents the grains from instantly rearranging in a tighter packing order (e.g., Kadau et al., 2009). This maintains a sparse, collapsible microstructure until cohesion is lost and suspends the slab in a metastable state. The slab material is assumed linear-elastic and deforming in plane strain relative to the z-direction. Extensive quantities are therefore given per unit length in z. The Young's modulus is denoted by E, and Poisson's ratio by ν. We assume that slab and substrate have comparable stiffness, so that the effect of the elastic mismatch is small. The load acting on the undisturbed weak layer is uniform and composed of a compressive (negative) stress $\sigma_\infty = -\varrho g h \cos\theta$ and a shear stress $\tau_\infty = \varrho g h \sin\theta$, where g is the acceleration of gravity.

We assume that the skier, positioned at $x = x_0$, acts as a line load $\vec{p}$ applied at a depth a of the snowpack (Fig. 1). This depth corresponds to the penetration depth of the skis (Jamieson, 1995). The slope-parallel and slope-normal components of the line load are denoted by

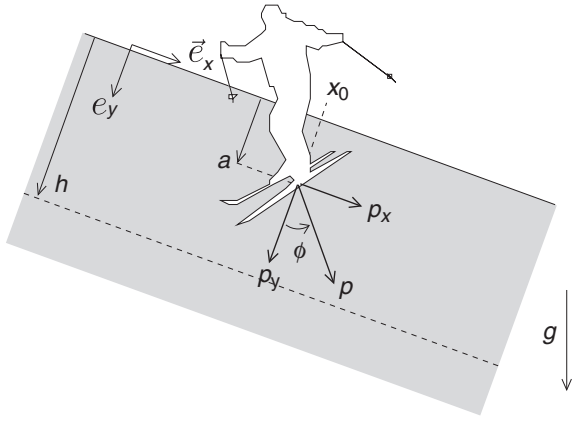

Fig. 1. A skier with position x_0 is assumed to sink into a slab of thickness h by an amount $a<h$. Under plain strain conditions, he/she acts as a line load with slope-parallel component p_x and slope-normal component p_y. The load causes an additional compressive stress $\sigma(x)$ and shear stress $\tau(x)$ at an arbitrary point in the weak layer plane.

p_x and p_y, respectively. The direction of loading is $\phi = \arctan(p_x/p_y)$. The static load p_0 of a motionless skier is typically around 400 N/m. Due to the accelerated motion while skiing, the instant magnitude $p = (p_x^2 + p_y^2)^{1/2}$ can be larger than p_0. The load causes a compressive stress $\sigma(x)$ and a shear stress $\tau(x)$ in the weak layer plane. Applying the superposition principle, the stress components can be partitioned into:

$$\begin{aligned} \sigma(x) &= \sigma_\infty + \sigma_\perp(x-x_0) + \sigma_\parallel(x-x_0) \\ \tau(x) &= \tau_\infty + \tau_\perp(x-x_0) + \tau_\parallel(x-x_0) \end{aligned} \tag{1}$$

where $\sigma_\parallel$ is the compressive stress in the weak layer plane exerted by an exclusively slope-parallel line load ($p_x \neq 0$, $p_y = 0$) and $\sigma_\perp$ is the compressive stress in the weak layer plane exerted by an exclusively slope-normal line load ($p_x = 0, p_y \neq 0$). The shear stresses $\tau_\parallel$ and $\tau_\perp$ are defined accordingly. The functions $\sigma_\perp$ and $\tau_\perp$ depend linearly on p_y, while the functions σ_{II} and $\tau_\parallel$ depend linearly on p_x. We note that $\sigma_\perp$ and $\tau_\parallel$ are even functions of their argument, while $\sigma_\parallel$ and $\tau_\perp$ are odd functions. For a linear isotropic slab material, $\sigma(x)$ and $\tau(x)$ are independent of the elastic modulus E of the slab. They can be estimated according to Melan (1932), as given in Appendix A and illustrated in the next section. An advantage of Melan's equation over previous load models (Salm, 1977; Föhn, 1987) is that the load can be applied both at the surface and inside the snowpack. This is, in accordance with ski penetration, more realistic than always applying the load on the surface. However, since the incision of the skier into the snowpack is not taken into account in Melan's equations, the accuracy of the calculation decreases with increasing penetration depth.

In order to determine the energy barrier for crack propagation in the weak layer under the action of a skier, we consider the stress intensity factors K_I and K_{II} associated with the tips of a mixed-mode anticrack of half-length r, located in the weak layer plane with center at $x = 0$ and loaded by $\sigma(x)$ in compression and by $\tau(x)$ in shear. We begin the analysis with the loading situation shown in Fig. 2a, in which a concentrated line force $q_x\vec{e}_x + q_y\vec{e}_y$ expressed in unit force per unit length acts on the crack faces at $x = x_1$. In mode I, in which $q_y > 0$ and $q_x = 0$, the solution is given by (e.g., Tada et al. 2001):

$$K_I\left(q_y, x_1\right) = \frac{q_y}{\sqrt{\pi r}}\left(\frac{r \pm x_1}{r \mp x_1}\right)^{\frac{1}{2}} \tag{2}$$

The upper sign of the $\pm$ operator refers to the crack tip on the right-hand side, the lower sign, to the crack tip on the left-hand side. For mode II, the same relation as for K_I applies, but q_y is replaced by q_x. The stress intensity factor for antimode I is obtained by reverting the sign of q_y. In common materials, this operation is not permissible as a reaction force to q_y immediately appears for $q_y < 0$. In cohesive-granular materials such as snow (Blackford, 2007),which are disposed to collapse in volume as the grain aggregate fails, the reaction force is delayed until tighter packing resists compaction. In practice, persistent weak snowpack layers collapse by one to several millimeters under fracture (van Herwijnen and Jamieson, 2005). This is enough

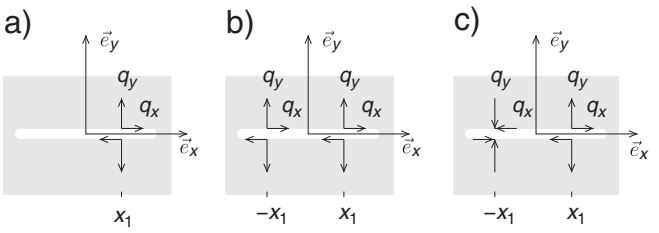

Fig. 2. Discrete loading of a crack of half-length r. (a) Unilateral line loading at $x = x_1$. (b) Symmetric loading at $x = \pm x_1$. (c) Antisymmetric loading at $x = \pm x_1$.

room for anticracks in the weak layer to become critical under typical loads before resistance to compaction sets in Heierli et al. (2008).

For symmetric line loading (Fig. 2b) and for antisymmetric line loading (Fig. 2c), the stress intensity factors are directly deduced by application of the superposition principle, $K^+ := K(q,x_1)+K(q,-x_1)$, respectively $K^- := K(q,x_1)+K(-q,-x_1)$. Thus:

$$K_I^+ = \frac{2q_y r}{\sqrt{\pi r(r^2-x_1^2)}},\quad K_I^- = \pm\frac{2q_y x_1}{\sqrt{\pi r(r^2-x_1^2)}}. \tag{3}$$

For K_{II}^+ and K_{II}^- in mode II, the same functional dependency holds, except that q_y is replaced by q_x. In order to obtain the stress intensity factors for an arbitrary distributed load, we decompose the distributed load into its symmetric and antisymmetric components, substitute these into Eq. (3), and integrate over x_1 from 0 to r:

$$K_I^+ = \sqrt{r/\pi}\int_0^r \frac{\sigma(x_1)+\sigma(-x_1)}{\sqrt{r^2-x_1^2}}dx_1, \tag{4}$$

$$K_I^- = \frac{\pm 1}{\sqrt{\pi r}}\int_0^r \frac{\sigma(x_1)-\sigma(-x_1)}{\sqrt{r^2-x_1^2}}x_1 dx_1, \tag{5}$$

For mode II, σ is replaced by τ. These expressions can be integrated numerically. In order to obtain simple analytical expressions, we observe that the integration is greatly simplified by expanding the distributed loads $\sigma(x)$ and $\tau(x)$ in a Taylor series around the crack center: $\sigma(x)=\sum \sigma_n x^n/n!$, $\tau(x)=\sum \tau_n x^n/n!$, $n=0,1,2...$, where $\sigma_n=\partial^n\sigma/\partial x^n|_{x=0}$ and accordingly for τ_n. We note that the summands with even power in x correspond to a symmetrical loading of the crack, whereas the terms with odd powers correspond to an antisymmetrical loading. Unequal contributions to the stress intensity factor of each crack tip apply to the case of antisymmetrical loading only. Using the superposition principle for K (i.e., $K_I=K_I^+ + K_I^-$, $K_{II}=K_{II}^+ + K_{II}^-$) and carrying out the integration we obtain:

$$\begin{aligned} K_I &= \sqrt{\pi r}\left(\sigma_0 \pm \frac{1}{2}\sigma_1 r + \frac{1}{4}\sigma_2 r^2 \pm \frac{1}{16}\sigma_3 r^3 + \ ...\right),\\ K_{II} &= \sqrt{\pi r}\left(\tau_0 \pm \frac{1}{2}\tau_1 r + \frac{1}{4}\tau_2 r^2 \pm \frac{1}{16}\tau_3 r^3 + \ ...\right). \end{aligned} \tag{6}$$

As previously, the upper sign of the $\pm$ operator refers to the crack tip on the right-hand side, the lower sign, to the crack tip on the left-hand side. For small crack half-width r, these expressions converge to $K_I=\sqrt{\pi r}\sigma_0$ and $K_{II}=\sqrt{\pi r}\tau_0$ and, in absence of a skier, to $K_I=\sqrt{\pi r}\sigma_\infty$ and $K_{II}=\sqrt{\pi r}\tau_\infty$. The higher order terms in the brackets improve on the accuracy of the calculation for $r>0$, but it is understood that $r \ll h$.

Using these expressions for K_I and K_{II} and assuming brittle fracture, the energy release rate G of the cracked system is obtained from the relation for plane strain $G=K_I^2/E' + K_{II}^2/E'$, where $E'=E/(1-\nu^2)$ (e.g., Tada et al., 2001). The energy release rate is computed for both crack tips, and the larger is retained. Thus, we assume the crack to expand if either one of its crack tips is unstable. We remark that the value of G both depends on crack size r and on skier position x_0 (through the intermediate of the Taylor coefficients). Therefore, in the worst case, the condition for crack propagation is:

$$\hat{G}(r,\vec{p}) = \max_{-\infty<x_0<+\infty}\{G(r,\vec{p},x_0)\} \geq w_f \tag{7}$$

where w_f is the fracture energy of the weak layer. Unlike Mahajan et al. (2010), we assume that the macroscopic energy release rate for the anticrack mode and for mode II are approximately equal (Heierli and Zaiser, 2008, Section 5.2). The value of r for which $\hat{G}(r,\vec{p})=w_f$ defines the critical half-length r_c under the load $\vec{p}$. The value of $\vec{p}$ for which $\hat{G}(r,\vec{p})=w_f$ defines the critical load $\vec{p}$ for a crack of half-length r. The value of x_0 which maximizes the middle expression for a fixed value of r and $\vec{p}$, defines the most effective position of the skier with respect to the crack.

Combined with Eq. (6), Eq. (7) provides a criterion for pre-existing flaws or cracks freshly induced by the skier to expand under the additional load exerted by the skier. This is the case when the half-width r_0 of the flaw or crack exceeds the critical half-width r_c resulting from Eq. (7). For loads typical of skiers, the present model leads to critical widths up to a few decimeter and down to a few centimeter. Our formalism thus requires that the weak layer material must be close to ideally brittle.

We note that the present skier model can be used not only to determine the stability of a mixed-mode anticrack but also to determine the stability of a simple shear crack. Simple shear cracking is contained as a limiting case in the model and is obtained by (i) forcing K_I to zero when the weak layer is not collapsible under fracture and (ii) applying residual crack face friction of the order of 0.6 times the local normal stress in the cracked weak layer (van Herwijnen and Heierli, 2009). Formally, this can be done by subtracting $0.6\sigma(x)$ from $\tau(x)$ in Eq. (1).

3. Illustration of the model

In order to illustrate the model, we consider the snowpack situation given in Table 1. We assume a skier of mass 70 kg on 1.70 m skis, exerting a static force $p_0 \cong 400$ N/m at a depth a of the snowpack. To begin with, we assume the force to act vertically. Fig. 3 shows the stress distributions σ and τ exerted by the skier in the weak layer plane. The three colors – black, red, and blue – in Fig. 3 correspond to different ski penetrations of $a/h=0$, 1/3, and 2/3, respectively, the four panels correspond to different slope angles $\theta=0, 30°, 45°$, and a theoretical 90°. The graphs show the compressive stress σ (full lines) and the shear stress τ (dotted lines). The width of the zone of influence of the skier in the weak layer plane – defined as full width at half peak value – is on the order of one meter for shallow penetration (Fig. 3). This finding is confirmed by field data measured by Schweizer and Camponovo (2001). The width of the zone decreases with increasing penetration depth and tends to increase with slope angle. The shape and range of the zone are very different for the induced shear component of stress and the induced compressive component of stress. In slopes up to about 60°, the shear component $\tau(x)$ is smaller in peak value but wider in range than that of the compressive component $\sigma(x)$, which is larger in peak value but narrower in range. The compressive component peaks almost directly under the skier near $x=x_0$, while the shear component peaks at two extrema of opposite sign on either side of the skier and goes through zero in between (N.B. see the fourth panel of Fig. 3 in which $\theta=90°$ for peaks of τ of the same sign and peaks of σ with opposite sign, indicating a zone of compressive stress with negative σ, and a zone of tensile stress with positive σ). Since we observe that, in skiable slopes, $\sigma_0^2 \gg \tau_0^2$ at the most effective position of the skier with respect to the crack (see Fig. 3), a large part of the energy to overcome the energy barrier for crack propagation comes from the compressive component exerted by the skier and only a small part from the shear component.

The stress calculations can be compared with field data in which the normal load exerted by a skier was measured with load cells (Schweizer et al., 1995). Applying Melan's model with the field data published therein, a skier of mass 70 kg, standing motionless atop of

Table 1
Snowpack characteristics for illustration of the skier triggering model.

ϱ [kg/m^3]	h [m]	E [Pa]	ν –	w_f [J/m^2]
200	0.50	4.0×10^6	0.25	0.1

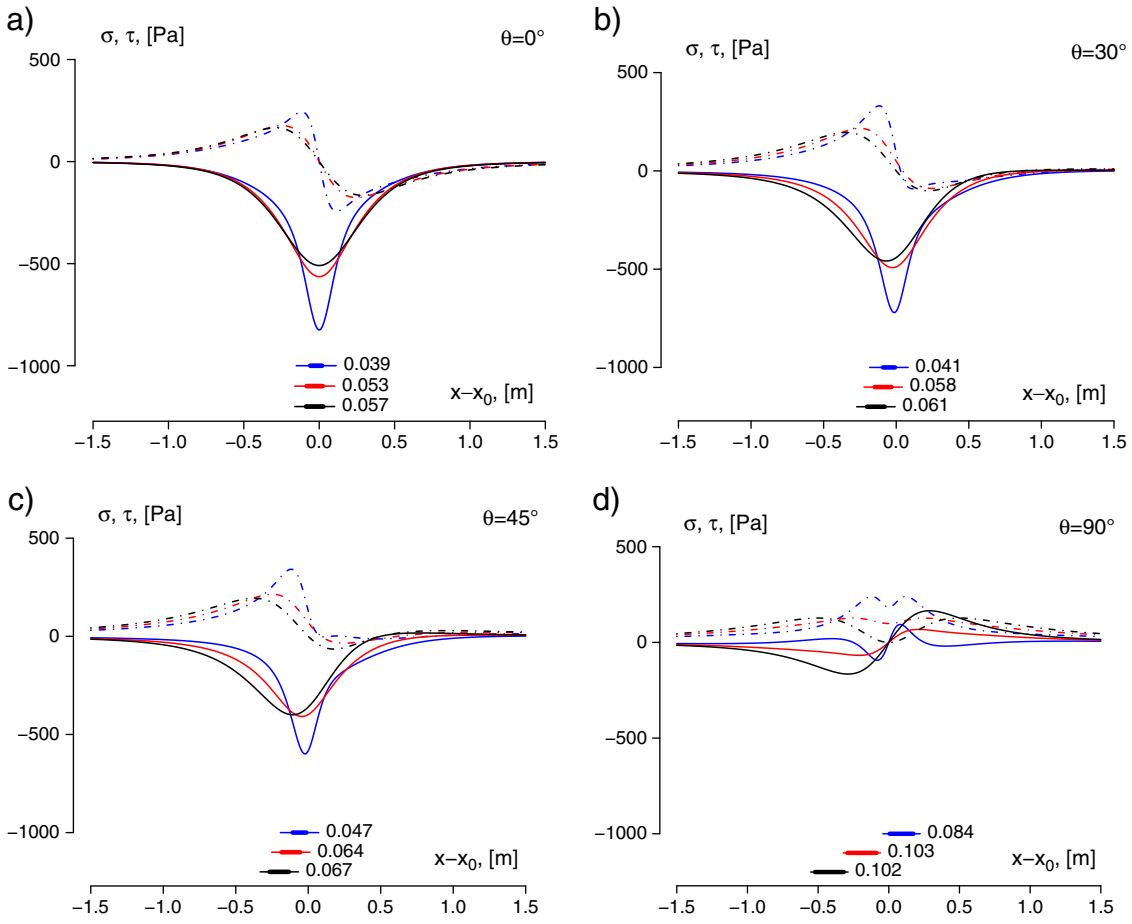

Fig. 3. Skier-induced stress components $\sigma-\sigma_\infty$ (full lines) and $\tau-\tau_\infty$ (dotted lines) in the weak layer plane. The colors represent ski penetration: $a/h=0$ (black), $a/h=1/3$ (red), $a/h=2/3$ (blue). The size and position of the critical crack are shown as thick colored segment. The juxtaposed figure indicates the critical half-length in meters. The thin segment indicates the critical size in the absence of the skier. (a) $\theta=0$, (b) $\theta=30$, (c) $\theta=45$, (d) $\theta=90$. Data: Table 1, $p=p_0=400$ N/m. Terms up to the first order in r were taken into account in Eq. (6).

the snowpack, sinking in by 0.11 m vertically above a load cell of dimensions 0.5 m×0.5 m=0.25 m^2, located at a depth of 0.48 m below the slab of density 180 kg/m^3, exerts an additional load of 105 N on the cell, which compares favorably with the measured 110 N. Based on the same field data, we find that the skier quickly flexing the knees corresponds to an increase of p by a factor of 1.6 compared to the static skier load p_0, whereas the skier jumping once corresponds to an increase of p by a factor of 2.2 with respect to p_0. These values give an estimation of the range in which p can be expected to vary during the action of skiing.

In Fig. 3, we show the critical crack widths as calculated with the present model. The thick segment indicates the critical size in the presence of the skier, while the thin segment represents the critical size in the absence of the skier. The printed figure is the critical half-width r_c in the presence of the skier (for comparison, the critical half-width without skier is in our example $r_c=0.13$ m). The skier reduces the critical width the most in horizontal terrain ($a=0$) and deep penetration ($a/h=2/3$), and the least in steep terrain ($\theta=90^\circ$) and shallow penetration ($a/h=0,1/3$). The position of the crack, as indicated on the graph, corresponds to the most effective position with respect to the skier. The steeper the slope, the more sideways the critical crack is located in relation to the skier, especially for shallow penetration. The pre-condition $r\ll h$ is satisfied in all cases.

In order to give a concrete example for critical skier loads, we assume that the largest flaw a skier will hit, in a day of skiing, has an expected size of $l_0=2r_0=0.08$ m in diameter. We ask whether this flaw remains stable or expands upon the passage of the skier. (If the mathematical expectation of the maximum flaw size were smaller than 0.08 m, the calculated critical load would be higher and reciprocally.) We thus substitute r_0 for r in Eq. (7) and calculate the critical load the skier must exert on the snowpack in order to trigger a flaw of this size. Also, we assume for simplicity that the thickness of the slab at different points of the snowpack is proportional to the cosine of the slope angle, $h\propto\cos\theta$. This corresponds to an idealized snowpack in which the snow has been deposited homogeneously without local drift snow accumulations. Using these assumptions, the dependency of the critical skier load with the slope angle is shown in Fig. 4. If the weak layer fails by propagation of a mixed-mode anticrack (full curves), the critical load to trigger the fracture process is virtually independent of slope angle up to angles of about 60°. In that range, the critical load slightly increases with slope angle, but the increase is very small and may be difficult to detect given the usual spatial fluctuations of the snow cover. In our example, the critical loads for avalanche-prone slopes between 30° and 45° are between one and two times the static line load of a typical skier and decrease with increasing penetration depth. For a slab of approximately half a meter in thickness, a penetration depth of 1/3 through the slab only marginally reduces the critical load with respect to no penetration. On the other hand, a penetration depth of 2/3 through the slab very substantially reduces the critical load by 40%. By contrast, if the weak layer were to fail by propagation of a simple shear crack (dotted curves), the critical loads to trigger fracture are much larger, between 7 and 20 times the static line load of a typical skier in the 30–45° window, and, importantly, rapidly decrease with increasing slope angle. In our example, the critical load decreases between 30° and 45° by a factor of 1.5 or more (Fig. 4, dotted curves).

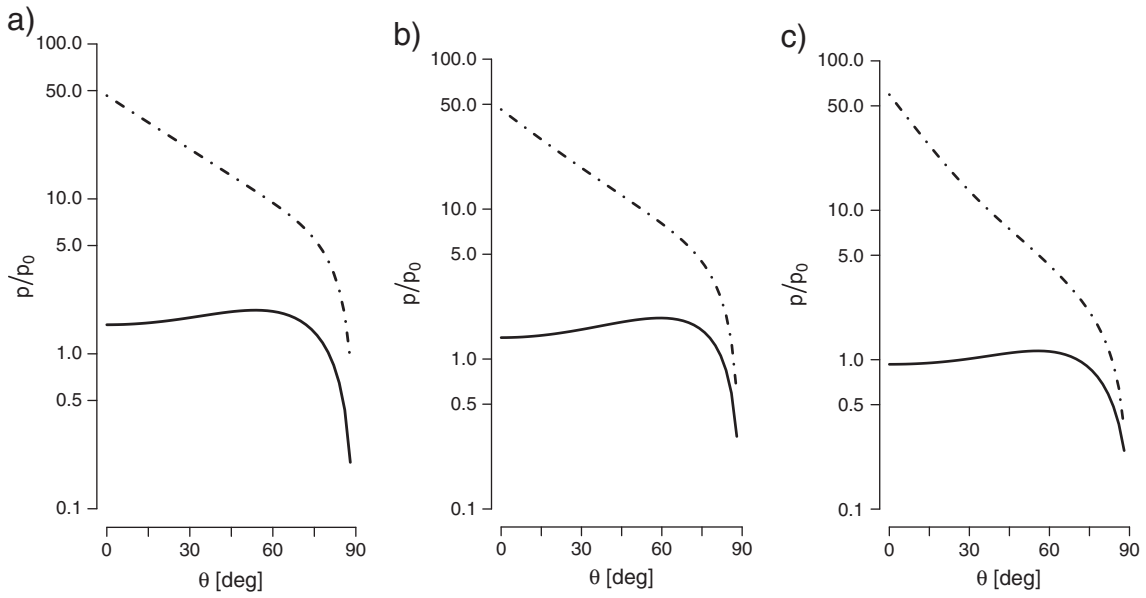

Fig. 4. Critical skier load in units of a typical load $p_0 = 400$ N/m, in terms of slope angle θ and for a flaw size of 0.08 m. (a) $a/h = 0$, (b) $a/h = 1/3$, (c) $a/h = 2/3$. Full line: critical load for mixed-mode anticrack. Dotted line: critical load for simple shear crack. In the scenarios (a) and (b), skiing sharply or jumping triggers anticracking; in scenario (c), anticracking is already triggered by the static load. The load is assumed to act vertically ($\phi = \theta$).

Thus, two contrary messages emerge from the comparison of the results: if the weak layer fails in anticrack mode, then fracture is not easier to trigger on steep slopes than on gentle slopes but equally or marginally more difficult. By contrast, if the weak layer fails in simple shear mode, then fracture becomes easier to trigger the steeper the slope. Since the finding that weak layer fracture is not necessarily easier to trigger in steep slopes than in gentle slopes relates to safe travel in avalanche terrain, we tested this proposition in field experiments.

4. Field experiments

In order to measure the difficulty of triggering fracture in a natural test sample, we utilized the "extended column test" method (ECT) and slightly modified the sample size (Simenhois and Birkeland, 2006). In addition to the ECT experiments, we used a layout in which the load is applied in the center of the sample and at various depths (Fig. 5). This layout is denoted by CECT for "centered" ECT. For both layouts, a vertical column of snow with rectangular base is isolated with a snow saw on all four sides from the surrounding snowpack. For ECT layouts, we cut to a size of $2h + 0.25$ m, but no less than 0.9 m, in cross-slope width, and to 0.3 m in the direction of the slope gradient. For CECT layouts, we cut to a cross-slope width of $4h + 0.11$ m. The reason to size the samples wider than usual is to reasonably reduce size and boundary effects, while compromising on the amount of preparation work for the samples under occasionally dangerous exposure. The samples are tested by placing the blade of a snow shovel (0.25 m in width) or a ski (0.11 m in width) flat on the column and vertically tapping on them repeatedly following a precise procedure in which the strength of the tapping is increased every ten taps (Simenhois and Birkeland, 2009; Greene et al., 2009) (Fig. 6). The number of taps until the sample fractures is recorded. This method is suitable for our issue since, like a skier, it tests the intact snowpack. For consistency in loading, the same observer conducted all the experiments of each measurement series.

The experiments were conducted on selected slopes in Colorado, Montana, and Alaska, USA, in which gentle changes in slope angle or

Fig. 5. CECT experiment. The test sample (contour enhanced) is cut free from the surrounding snowpack. A small trench of variable depth and fitting the ski is dug into the center of the sample. Fracture in the weak layer is initiated by tapping on the ski.

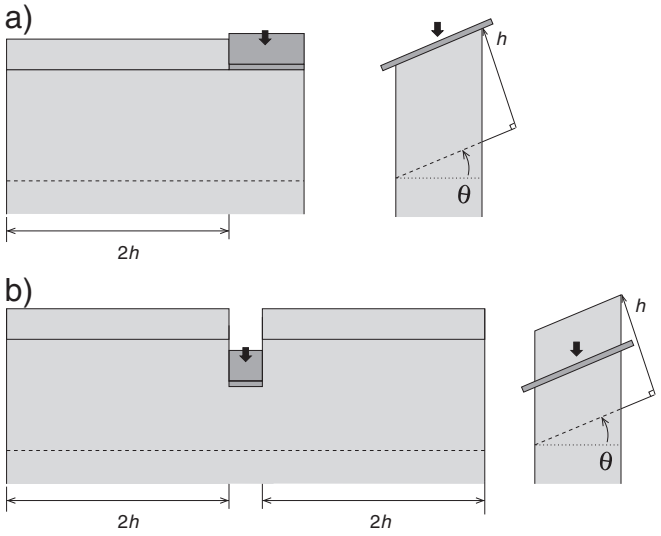

Fig. 6. (a) ECT experiment. (b) CECT experiment. The test sample (light grey) is cut free from the surrounding snowpack. In case (a), the blade of a snow shovel is placed on top at one edge (dark grey) and tapped according to prescriptions (black arrow). In case (b), a ski is used instead of the shovel. Tapping is stopped when the weak layer (dashed line) fractures. The test score is ECTP/CECTP if the weak layer fractured from one end of the sample to the other at one go.

rollovers allowed for sampling a variety of slope angles with minimal changes in snow structure. Altogether, the slope angles ranged from 7° to 44° (Table 2). On one slope in Alaska the observers roped up to improve safety while conducting the tests. Sighting upslope on the snow surface with a Suunto clinometer prior to each test allowed us to quantify slope angles to an accuracy of $\pm 1°$. Almost all experiments were conducted immediately adjacent to each other in the uphill direction in order to reduce spatial variations from one sample to the other. The structure of the snowpack was reasonably consistent at the test sites. The characteristic data are given in Table 2. In dataset 1 to 4, the weak layer consisted of buried surface hoar crystals with crystal sizes varying from 4 to 10 mm on the different slopes, while in datasets 5 and 6 the slab rested on a thin layer of facets. For our analysis, we only considered experiments in which the sample fractured at one go across the entire column on the weak layer of interest (a score denoted as ECTP or CECTP, respectively, where *P* stands for 'propagate').Thus, two experiments in dataset 1 for which the samples fractured on a layer of depth hoar on the ground were discarded. The snowpack at test site 4 was challenging due to the presence a second layer of buried surface hoar that occasionally fractured. Altogether, 18 of a total of 32 experiments at test site 4 fully fractured on the surface hoar layer of interest (i.e., classified as ECTP), and this subset was used for our analysis. In the datasets 2, 3, 5, and 6, all experiments were used for our analysis, as all samples fully fractured at one go on the layer of interest. Dataset 6 was obtained by placing the ski at various depths of the snowpack before tapping. To this end, a small trench was dug into the center of the sample, just wide enough to hold the ski (Fig. 5). Varying depth a of the trench allowed us to investigate the effect of ski penetration on triggering fracture.

The results from datasets 1 to 5 show that the number of taps required to fracture the weak layer remained reasonably constant, or increased slightly, with increasing slope angle (Fig. 7). For dataset 1, ECT scores varied from 12 taps to 16 taps. There is a slight tendency toward an increasing number of taps on the steeper parts of the slope. Dataset 2 was collected 2 days later and on the same slope as dataset 1. The results are again consistent, ranging from 12 taps to 15 taps. Like the previous dataset, there is a slight tendency toward an increasing number of taps with slope angle. Dataset 3 covers the smallest range of slope angles, varying from 38° to 43°. The ECT scores were either 12 taps or 13 taps at all locations, and no trend appears for these data. We investigated the steepest slopes at test site 4, where a large rollover allowed us to sample from 30° to 44°. This dataset has the largest range of ECT scores, ranging from 12 taps to 22 taps, and shows a stronger increase with steepness. Below 39°, all ECT scores were 14 taps or less. Above 39°, all ECT scores were 15 taps or more. Dataset 5 also samples a large range of slope angles, from 12° to 32°. The CECT score gradually increases by five taps as the slope angle increases by 20°. In summary, none of the five datasets shows a tendency for a decreasing number of taps with increasing slope angle.

The results from dataset 6 show that the number of taps required to fracture the weak layer decreases as the penetration depth increases (Fig. 8). We also observe that, for shallow penetration ($a/h = 0$), the number of taps always exceeded 20 when fracture initiated. That is, the taps were hit from the shoulder according to ECT prescriptions. For deep penetration instead ($a/h \geq 1/3$), the number of

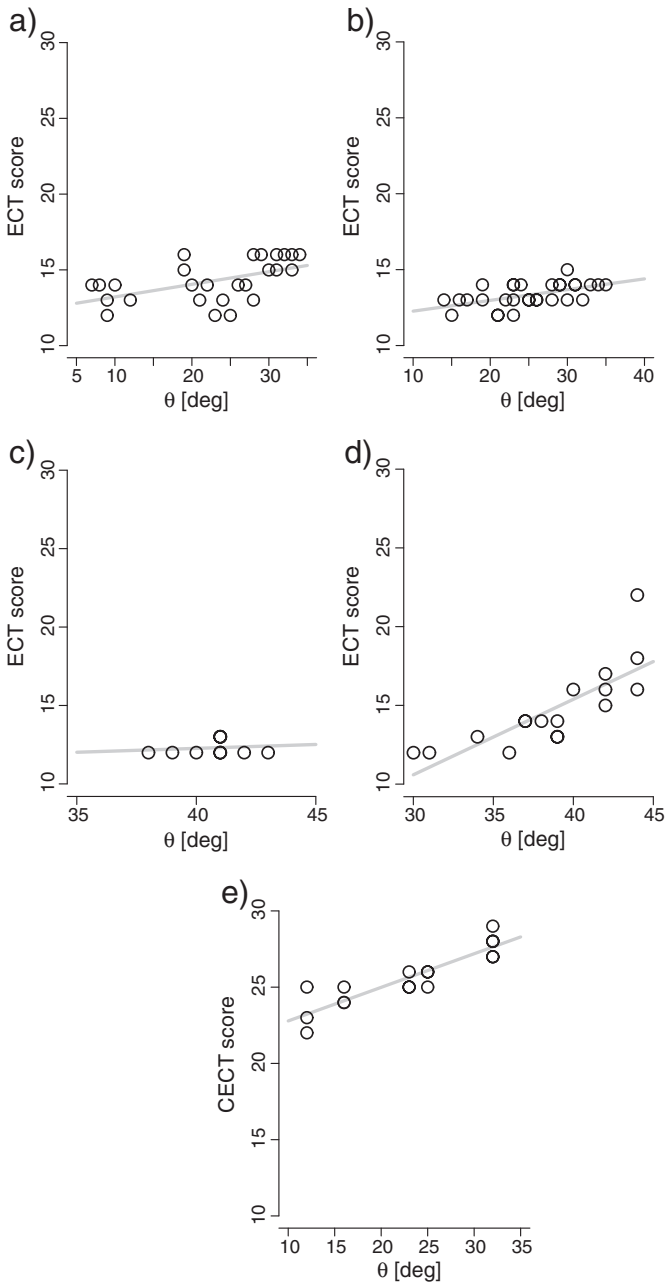

Fig. 7. ECT scores in number taps versus slope angle θ. (a) Dataset 1, (b) dataset 2, (c) dataset 3, (d) dataset 4, (e) dataset 5. The grey lines represent linear regression.

Table 2
Geographical location and snowpack characteristics of field experiments. *N*: number of experiments, *F*: weak layer crystal type (SH: surface hoar, FC: facets), *e*: weak layer grain size. Other symbols as defined in Section 2. Uncertainty on last digit in brackets (standard deviation).

Set	Mountain range	Type	N [–]	θ [°]	$\langle h \rangle$ [m]	$\langle a \rangle$ [m]	ϱ [kg/m^3]	F [–]	e [mm]
1	Henry, MT	ECT	26	7–34	0.27 (1)	NA	180	SH	4–8
2	Henry, MT	ECT	30	14–35	0.30 (2)	0.13	180	SH	4–8
3	Chugach, AK	ECT	10	38–43	0.24 (1)	0.11	NA	SH	6–10
4	Chugach, AK	ECT	18	30–44	0.27 (4)	NA	160	SH	4–6
5	Copper, CO	CECT	18	12–32	0.38 (3)	0.01	300	FC	0.5–1
6	Copper, CO	CECT	42	12–32	0.38 (3)	Variable	300	FC	0.5–1

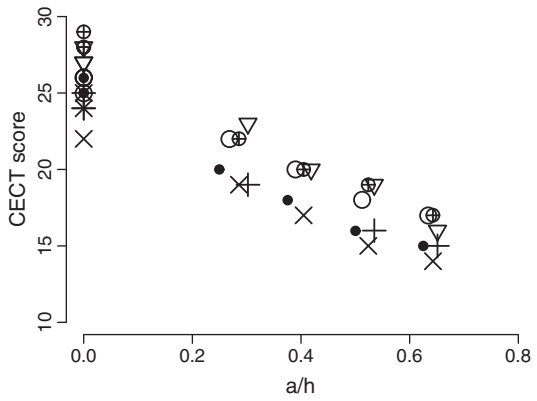

Fig. 8. Decrease of CECT score with increasing ski penetration a/h. The six symbols represent measurement series at six different locations in the test slope.

taps was always less than 20 when fracture initiated. In this case, the taps were hit from the elbow. Thus, not only the number of taps decreased with increasing penetration depth but also the magnitude of the tapping force.

5. Discussion

In Section 2, we derived a criterion for a crack or flaw to expand under the action of a skier. We left aside the question whether or not the skier induces cracks in seemingly intact portions of the weak layer.

A few assumptions were used to build the theoretical model. Firstly, the model is based on the linearity and isotropy of the slab material, allowing for the superposition principle to be applicable. This principle is used (i) in Melan's equations for the stress field exerted by a skier in the snowpack, (ii) to add the stress fields due to the slope-parallel and slope-normal components of the skier load, and (iii) to determine the stress intensity factors for distributed loads on the crack faces. The comparison with field measurements collected by Schweizer et al. (1995) in Section 3, which shows a difference of 5% for the average stress on the load cell, indicates that this approximation is acceptable. Secondly, the skier load is modeled as a single line force. In a linear material, the load can, in principle, easily be modeled as a surface load, corresponding to one ski, or as a double line load, respectively, a double surface load corresponding to two skis. However, there is no advantage in doing so since the skis are often pressed into the snow with unequal force, so that one ski prevails over the other. In addition, as we shall see, the single line load situation appropriately corresponds to a worst-case scenario for triggering. We note that modeling the ski as a line force limits the model to penetration depths on the order of approximately one or two ski widths away from the weak layer.

Another assumption we used is that the granular aggregate constituting the weak layer fails by brittle fracture, a case that is well supported for dry snow (e.g., Narita, 1980; Kirchner et al., 2004) and references therein). Others regard dry snow as a quasi-brittle material (Bazant et al., 2003). Accordingly, a finite fracture process zone should be taken into account in the modeling. However, so far no reliable measurements of the finite size of a plastic zone embedding the crack tip exist for natural weak layers. Therefore, until dependable proof for the existence and the size of a process zone is available, brittle fracture remains the most plausible fracture mechanism for skier triggering in dry snow.

We further assumed that both the shear stress τ and the normal stress σ are interrupted across the anticrack, as the granular debris in the cracked weak layer is neither compressed nor sheared in the course of compaction. Thus, although the same friction law applies during collapse and after completed collapse, the amount of friction is 0 in the first case (because $\sigma(x) \equiv 0$ between the anticrack faces) and $\mu\sigma(x)$ in the second, where $\sigma(x) \neq 0$ and $\mu \approx 0.6$ (van Herwijnen and Heierli, 2009). In fact, field experiments indicate that friction drops to a small residual value during the collapsing phase, but not exactly to zero (van Herwijnen and Heierli, 2009). Thus, some amount of friction should be associated with anticracks even during the course of collapse. However, the experimental values for the residual friction are small throughout and therefore neglected in the present formulation. The calculated critical anticrack sizes therefore indicate the smallest possible values (corresponding to the worst case).

The model distinguishes between the effect of the slope-normal and slope-parallel components of the skier on triggering fracture in the weak layer. The load causes a compressive component $\sigma(x)$ and a shear component $\tau(x)$ of the stress tensor in the fracture plane. We have seen in Section 3 that the shape, range, and value of $\sigma(x)$ and $\tau(x)$ are different. Given flaws, microcracks, or other sharp heterogeneities in the weak layer, a critical load can be associated to each flaw of known size. The critical load depends on the direction of loading. Assuming the load to act vertically and assuming a spatially homogeneous snowpack deposited without wind accumulations, the critical load for anticracking remains constant (or increases very slightly) with increasing slope angle until about 60° (Fig. 4). In this case, the difficulty of triggering fracture remains virtually constant with slope angle. If the weak layer fails in simple shear mode instead, the critical load decreases monotonically and rapidly with increasing slope angle (Fig. 4). In that case, it becomes gradually easier to trigger fracture with increasing slope angle. Approaching a theoretical 90°, the shear crack and anticrack models converge.

The influence of the loading direction ϕ is shown in Fig. 9 for a slope of 40°. The graph shows a broad minimum for the critical load. The most effective loading direction is not far from slope-normal ($\phi = 0$), and the least effective directions are the slope-parallel directions $\phi = +90^{\circ}$ and $\phi = -90^{\circ}$. These results remain qualitatively valid for other, skiable slope angles and emphasize the major role of the compressive stress in the failure of the weak layer.

The field experiments show that triggering fracture in the weak layer by conducting an ECT takes the same number of taps or slightly more taps as the slope angle increases (Fig. 7). The results are similar across all four ECT datasets, as well as one CECT dataset. Of course, a dynamical and not yet fully understood mechanical process causes fracture to initiate in ECT experiments. However, comparative field experiments indicate that an increasing ECT score goes in concert with a higher stability against skier triggering (Simenhois and Birkeland, 2009). In addition, field data obtained by another, static method for fracture initiation show the same trend with slope angle (Gauthier and Jamieson, 2008). In those experiments, fracture across

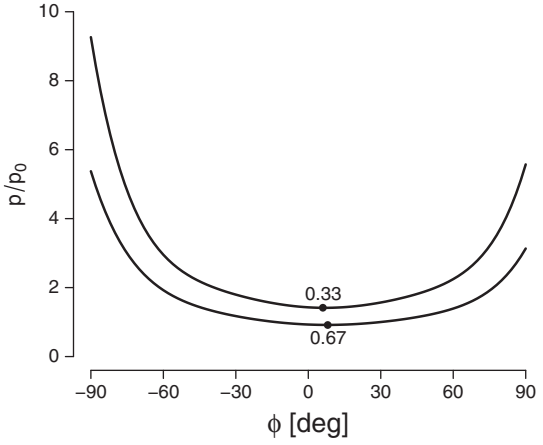

Fig. 9. Critical skier load in units of a typical load $p_0 = 400$ N/m, in terms of load direction ϕ. The slope angle θ is 40 . The figures indicate the relative penetration depth a/h. The graph indicates that the triggering of fracture is distinctly easier under compressive loads ($\phi = 0$) than under shear loads ($\phi = \pm 90$). Data are as in Fig. 4.

the entire test sample is initiated statically by saw-cutting into the weak layer from an edge until the crack tip ahead of the saw becomes unstable and propagates. Regarding the traditional rutschblock test, Campbell and Jamieson (2007) obtained significant negative correlation of rutschblock stability scores with slope angle for only 2 out of 9 series of experiments (p-value: 0.05), while the remaining 7 series are non-significant or positive and conform to our field data. The bottom line is that different kinds of field experiments confirm the theoretical expectation for anticracks that fracture is equally or more difficult to trigger in the weak layer as the slope angle increases, regardless of the method to initiate fracture. We note that other results have been obtained in the past. Jamieson and Johnston (1993) found significant negative trends in 10 of 24 rutschblock datasets, concluding that rutschblock scores decreased on steeper slopes. However, in the remaining 14 datasets, no significant trend existed. Jamieson (1999) suggested a decrease of approximately 1 tap in the compression test scores for each 10° increase in slope angle based on finding a significant trend in 7 of 11 datasets. The decrease was attributed to snowpack variability and not to increasing shear stress with slope angle.

Another aspect of our interpretation of the field data is the spatial variability of the snowpack (Simenhois and Birkeland, 2009). In our field experiments, the test sites were carefully selected to ensure a small spatial variability of the mechanical properties of the slab across the area. Nevertheless, spatial variability of some kind almost certainly remained. However, the probability to find a non-decreasing difficulty of triggering the weak layer by chance in 5 series is a priori $1-(1/2)^5 \approx 0.97$. Therefore, the confidence that the result is not obtained purely by chance is rather high.

We interpret these results as a strong indication that persistent weak layers fail by propagation of mixed-mode anticracks and not by propagation of simple shear cracks. Both the shear load to shear strength ratio ("stability index") and the fracture mechanical simple shear models predict a decreasing difficulty of triggering fracture in steeper slopes (Fig. 4). Since the field data show otherwise, we infer that these approaches are unsuitable for understanding the failure of persistent weak layers.

On a practical note, one may ask what strategies skiers can employ to reduce the risk of triggering fracture. The best strategy among all, of course, is to identify and avoid suspect slopes. Besides this, the calculations indicate two complementary strategies. Firstly, Figs. 3 and 9 signal that any technique that reduces the peak slope-normal load, and, in accordance with established experience (Jamieson and Johnston, 1998), reduces the penetration depth into the slab also reduces the odds of triggering fracture. This result is consistent with observations from ski guides in Alaska and elsewhere who have noticed that skiing light and fast, making long, arcing turns is less likely to trigger an avalanche than making sharp, bouncy turns. Secondly, Fig. 10 signals that the width of the stance and the load distribution on the skis significantly affect the critical crack length: a skier alternately loading one ski and then the other, e.g., during downhill turns or when travelling uphill with climbing skins, represents the worst scenario in the sense that the critical half-width is the smallest when the load is entirely on one ski (Fig. 10a). Spreading the skis by half a meter (a rather wide but reasonable stance) and loading them equally increase the critical length by as much as 30% (Fig. 10b). Increasing the spread to 1 m and still loading the skis equally, the critical length would increase by another 10% (in Fig. 10c). Spreading the skis any further is neither practicable and nor does it increase the critical crack size substantially (Fig. 10d). These figures are obtained for equal penetration depth. Thus, by spreading the skis half a meter apart (or slightly more if the skier is comfortable with it) and paying attention to loading both skis evenly, the risk of triggering fracture is decreased. Nevertheless, we emphasize that,

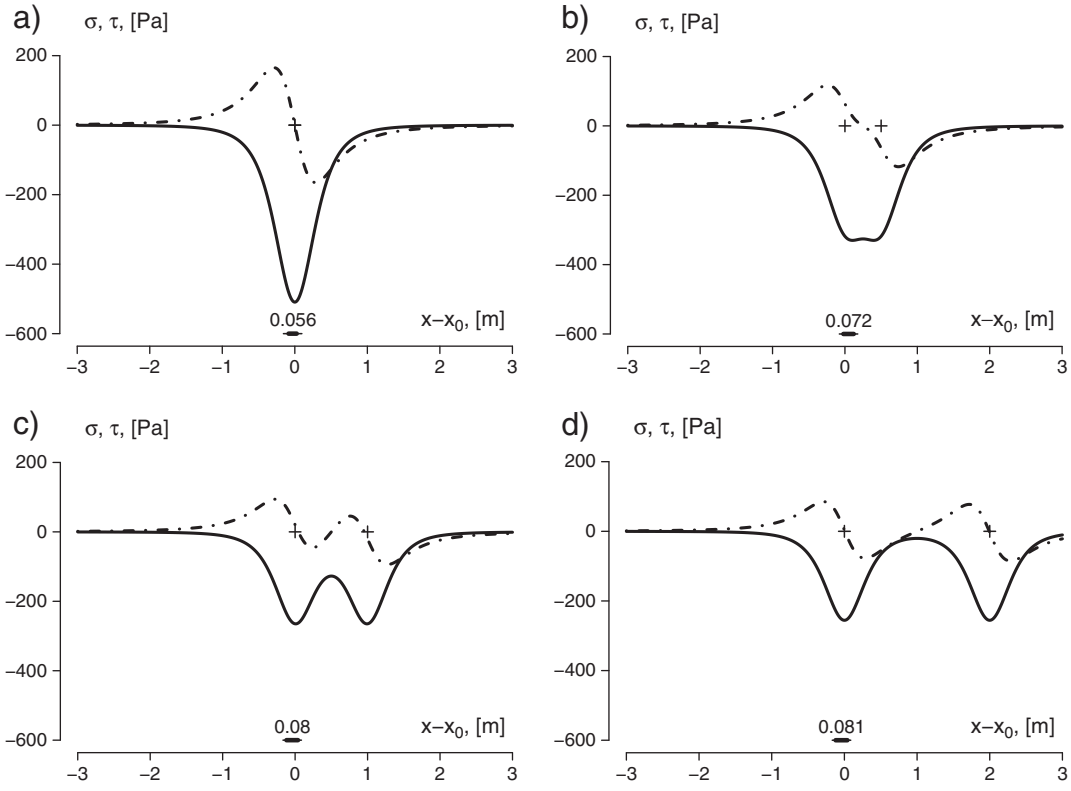

Fig. 10. Influence of spreading the skis apart and loading them evenly. (a) Loading all weight on one ski, (b) spreading the skis 0.5 m apart and loading them evenly, (c) skis 1 m apart, evenly loaded, (d) spreading the skis more than 1 m apart does not increase the critical crack size substantially. The result is shown for $\theta = 0$ and $a/h = 0$ but remains qualitatively valid for all slope angles and deeper penetration. The dots indicate the x-position of the loads. Data: see Table 1. Symbols are as in Fig. 3.

depending on the skier's aptitude, taking a wider stance can increase the difficulty of skiing steep slopes. If using the technique is likely to result in a fall, its use is counter-productive.

A second implication of Fig. 10 is that the interaction of loads more than 2 m apart is negligible regarding the effect on critical crack size. Thus, a couple of meters' distance between the skiers implies virtually no greater risk than the sum of the risks, taken individually. If the distance is closer than 1 m, the interaction between the skiers decreases the critical crack size substantially and therefore increases the odds of triggering fracture. Thus, the model reproduces the well-known precaution that skiers in avalanche terrain or in any location where fracture can be triggered should not group too closely.

Clearly an increase of the critical crack length decreases the risk of triggering fracture under equal loads, but is the decrease in risk substantial? In order to outline the answer, we consider a persistent weak layer of surface hoar with typically $\lambda = 150\ \mathrm{m}^{-1}$ supporting bonds per unit length. Assuming the bonds to be positioned randomly, the probability $P(l)$ of a defect of length $l = 2r$ or more is $P(l) = e^{-\lambda l}$. The average distance $d(l)$ to be covered by the skier to hit a defect of length l or more is therefore $d(l) = (\lambda P(l))^{-1} = e^{\lambda l}/\lambda$. In order to compare the risks involved with scenarios of different critical lengths, such as alternately loading one ski then the other (Fig. 10a, $l_1 \approx 0.11$ m) or loading the skis evenly and taking a stance of half a meter (Fig. 10b, $l_2 \approx 0.14$ m), we find $d(l_2) : d(l_1) = e^{\lambda(l_2 - l_1)}$. In our example $d(l_2) : d(l_1)$ is on the order of 100:1. That is, if the skier covers the same terrain in both cases, he or she is on the order of 100 times less likely to trigger fracture in the second scenario than in the first. This simple analysis indicates that even a small increase of the critical crack length can be a very substantial element of risk evaluation.

The results question the traditional understanding that steeper slopes are more dangerous because of easier fracture initiation, since, given similar snow structure, fracture appears to be equally difficult or even more difficult to initiate in steeper terrain. We think that the true reason that steep slopes are dangerous is because it is more likely on steep slopes to overcome the residual contact forces between the freshly debonded slab and the basal plane, as well as the contact forces at the periphery of the debonded slab. Thus, the steeper the slope, the greater the odds of releasing an avalanche. The gentler the slope, the greater the odds of releasing an alarming, but harmless whumpf instead (unless it propagates far enough to release a remote avalanche). In this sense, the perception of steep slopes being dangerous to ski remains valid.

Using a pragmatic approach, one can employ the present method to investigate possible skier triggering scenarios given a broad knowledge of snowpack conditions. In order to obtain a relative ranking of a selection of scenarios by the difficulty of skier triggering, two schemes are possible: (i) either one ranks the scenarios by the value of r_c given p (lowest r_c indicating lowest stability) or (ii) one ranks the scenarios by the value of p_c given r_0 (lowest p_c indicating lowest stability). In both schemes, the critical level is determined by Eq. (7).

6. Conclusion

In the present work, a mathematical model of skier triggering based on the principles of mixed-mode anticracking is proposed. The model can be used to determine the critical size of a crack in the prospective fracture plane under loads like those exerted by skiers. Combined with empirical data on flaw sizes, the model may be employed to assess the snowpack stability associated with potential skier triggering scenarios.

According to the model, the combination of a small number of factors increases the risk of triggering fracture: the intensity and the direction of the skier load, the depth of the weak layer, the stiffness and penetrability of the slab, the fracture energy of the weak layer, and the size of flaws. Depending on the snowpack conditions and the route chosen by the skiers, the combination of these factors is more or less likely to occur.

Regarding how load superposition alters the risk of triggering fracture, we find that if two skiers gather closely, they substantially decrease the critical size for which a crack starts to propagate. According to the calculation, approaching each other by less than about 1 m increases the triggering risk, while remaining apart by a couple of meters or more implies virtually no greater risk than the sum of the risks taken individually. This confirms that parties should not gather too closely (e.g., for reading a map). Of course, it remains wise to only expose one skier at a time on potential avalanche slopes to eliminate the chances of being caught in the same avalanche.

The present model of skier triggering confirms strategies for traveling on potentially dangerous terrain, if unavoidable (e.g., during a rescue): the skier should avoid all actions that increase the instantaneous load (especially the slope-normal component) and penetration depth, such as falling, jumping, wedelling, decelerating, and alike. In addition, taking a wider stance and equally dividing the load on both skis increases the critical length and therefore decreases the risk of triggering fracture. The model also explains why any actions that load the skis very unequally, such as travelling uphill with climbing skins, can trigger avalanches even though they involve small dynamic loads.

A major practical result of the present work is that, given similar snowpack conditions, fracture is equally difficult to trigger on steep and gentle slopes. The tendency of an increasing difficulty with increasing slope angle is marginal and not practically relevant. While most practitioners know that fracture can be triggered on low-angle slopes and anticipate the consequences, it is not commonly realized that fracture can be triggered as easily on low angle slopes as on steeper ones. On the contrary, critical loads are often presumed to decrease with increasing slope, a perception that conceptually emerges both from the classical stability index and from the shear models of weak layer fracture: mathematically, both indicate that the critical loads decrease with increasing slope angle. Due to the obvious practical reach for safe travel of this new paradigm, we validated this result experimentally in the field. The experimental results mirror those of the model and show that triggering fracture in a weak layer is equally or slightly more difficult on steep slopes in comparison with gentler slopes. Field data obtained by another method for fracture initiation also show the same trend with slope angle. We therefore advise skiers to be aware that triggering fracture can be equally easy in a 30° slope than in 45° slope and not invariably more difficult in a gentle slope than in a steep slope, as implied by the traditional views supported by the shear model and the stability index.

The field data indicate that there is a fundamental lack of understanding in the traditional approaches of skier triggering, whether based on a shear stress to shear strength ratio ("stability index") or on simple shear cracking models. These models indicate a false trend for the difficulty of triggering fracture in persistent weak layers in terms of slope angle. Instead, the present model provides a new framework to understand skier triggering of slab avalanches, which is in accordance with the field data at hand.

From an operational perspective, the results show that, as long as the snow structure remains reasonably consistent in space, snowpack observers can conduct dependable tests on persistent weak layers in gentler, safer terrain before committing themselves to exposed areas. This is only possible when failure is propagated by anticracks, since shear cracks cannot develop in the low-angle terrain.

Acknowledgments

Financial support by the DFG project Gu367/30 is gratefully acknowledged. We thank Theo Meiners and Alaska Rendezvous Guides for providing field access and logistical support for the Alaska field work and the Gallatin National Forest Avalanche Center for logistical support

for the Montana field work. Field work assistance from Jessica Baker, Matt Borish, and Zach Guy was much appreciated.

Appendix A

According to Melan (1932), the components of the stress tensor generated by a line load in a homogeneous, isotropic material in a half-space are:

$$\sigma_{\perp}(x) = p_y\left\{\frac{\alpha}{\pi}\left[\frac{(h-a)^3}{r_1^4} + \frac{(h+a)\left[(h+a)^2+2ah\right]}{r_2^4} - \frac{8ah(h+a)x^2}{r_2^6}\right] + \frac{\beta}{\pi}\left[\frac{h-a}{r_1^2} + \frac{3h+a}{r_2^2} - \frac{4hx^2}{r_2^4}\right]\right\},$$

$$\tau_{\perp}(x) = p_y x\left\{\frac{\alpha}{\pi}\left[\frac{(h-a)^2}{r_1^4} + \frac{h^2-2ah-a^2}{r_2^4} + \frac{8ah(a+h)^2}{r_2^6}\right] + \frac{\beta}{\pi}\left[\frac{1}{r_1^2} - \frac{1}{r_2^2} + \frac{4h(a+h)}{r_2^4}\right]\right\},$$

$$\sigma_{\parallel}(x) = p_x x\left\{\frac{\alpha}{\pi}\left[\frac{(h-a)^2}{r_1^4} - \frac{a^2-h^2+6ah}{r_2^4} + \frac{8ahx^2}{r_2^6}\right] - \frac{\beta}{\pi}\left[\frac{1}{r_1^2} - \frac{1}{r_2^2} - \frac{4h(a+h)}{r_2^4}\right]\right\}$$

$$\tau_{\parallel}(x) = p_x\left\{\frac{\alpha}{\pi}\left[\frac{(h-a)x^2}{r_1^4} + \frac{(a+h)\left(2ah+x^2\right)}{r_2^4} - \frac{8ah(a+h)x^2}{r_2^6}\right] + \frac{\beta}{\pi}\left[\frac{h-a}{r_1^2} + \frac{3h+a}{r_2^2} - \frac{4h(a+h)^2}{r_2^4}\right]\right\},$$

where

$$\alpha = \frac{\nu}{2}\left(\frac{1}{\nu}+1\right), \quad r_1 = \sqrt{(h-a)^2+x^2},$$

$$\beta = \frac{\nu}{4}\left(\frac{1}{\nu}-1\right), \quad r_2 = \sqrt{(h+a)^2+x^2}.$$

The variables are as defined in Section 2.

References

Bazant, Z.P., Zi, G.S., McClung, D., 2003. Size effect law and fracture mechanics of the triggering of dry snow slab avalanches. J. Geophys. Res. 108 (B2), 2119.

Blackford, J.R., 2007. Sintering and microstructure of ice: a review. J. Phys. D 40, R355–R385.

Campbell, C., Jamieson, B., 2007. Spatial variability of slab stability and fracture characteristics within avalanche start zones. Cold Reg. Sci. Technol. 47, 134–147.

Fletcher, R.C., Pollard, D.D., 1981. Anticrack model for pressure solution surfaces. Geology 9, 419–424.

Föhn, P.M.B., 1987. The stability index and various triggering mechanisms. Proc. Davos Symposium, Avalanche Formation, Movement and Effects, Davos, Sept. 1986: IAHS Publ., 162, pp. 195–214.

Gauthier, D., Jamieson, B., 2008. Evaluation of a prototype field test for fracture and failure propagation propensity in weak snowpack layers. Cold Reg. Sci. Technol. 51 (2–3), 87–97.

Greene, E.M., et al., 2009. Snow, Weather, and Avalanches: Observational Guidelines for Avalanche Programs in the United States. American Avalanche Association, Pagosa Springs, Colorado. 150 pp.

Heierli, J., Zaiser, M., 2008. Failure initiation in snow stratifications containing weak layers: nucleation of whumpfs and slab avalanches. Cold Reg. Sci. Technol. 52 (3), 385–400.

Heierli, J., Gumbsch, P., Zaiser, M., 2008. Anticrack nucleation as triggering mechanism for slab avalanches. Science 321 (5886), 240–243.

Jamieson, B., 1995. Avalanche prediction for persistent snow slabs. PhD thesis, University of Calgary, Department of Civil Engineering.

Jamieson, B., 1999. The compression test—after 25 years. Avalanche Rev. 18 (1), 10–12.

Jamieson, J.B., Johnston, C.D., 1993. Rutschblock precision, technique variations and limitations. J. Glaciol. 39 (133), 666–674.

Jamieson, J.B., Johnston, C.D., 1998. Refinements to the stability index for skier-triggering of slab avalanches. Ann. Glaciol. 26, 296–302.

Kadau, D., Andrade, J.S., Herrmann, H.J., 2009. Collapsing granular suspensions. Eur. Phys. J. E 30 (3), 275–281.

Kirchner, H.O.K., Peterlik, H., Michot, G., 2004. Size independence of the strength of snow. Phys. Rev. E 69 (1), 011306.

Lawn, B., 1993. Fracture of Brittle Solids, second edition. Cambridge University Press, Cambridge, New York, Melbourne.

Mahajan, P., Kalakuntla, R., Chandel, C., 2010. Numerical simulation of failure in a layered thin snowpack under skier load. Ann. Glaciol. 51 (54), 169–175.

McCammon, I., Haegeli, P., 2006. Evaluation of a rule-based decision aid for recreational travelers in avalanche terrain. Proc. Int. Snow Science Workshop, Telluride, Colorado, Oct. 1-6.

Melan, E., 1932. Der Spannungszustand der durch eine Einzelkraft im Innern beanspruchten Halbscheibe. Z. Angew. Math. Mech. 12, 343–346.

Narita, H., 1980. Mechanical behavior and structure of snow under uniaxial tensile stress. J. Glaciol. 26 (94), 275–282.

Salm, B., 1977. Snow forces. J. Glaciol. 19 (81), 67–100.

Schweizer, J., Camponovo, C., 2001. The skier's zone of influence in triggering slab avalanches. Ann. Glaciol. 32, 314–320.

Schweizer, J., Camponovo, C., Fierz, C., Föhn, P.M.B., 1995. Skier triggered slab avalanche release—some practical implications. Proc. Int. Symposium: Sciences and mountain, Chamonix, May 30–June 3, pp. 309–315.

Simenhois, R., Birkeland, K., 2006. The extended column test: a field test for fracture initiation and propagation. Proc. Int. Snow Science Workshop, Telluride, Colorado, Oct. 1–6.

Simenhois, R., Birkeland, K., 2009. The extended column test: test effectiveness, spatial variability, and comparison with the propagation saw test. Cold Reg. Sci. Technol. 59 (2–3), 210–216.

Tada, H., Paris, P.C., Irwin, G.R., 2001. The Stress Analysis of Cracks Handbook. AMSE Press, New York.

van Herwijnen, A., Heierli, J., 2009. Measurement of crack-face friction in collapsed weak snow layers. Geophys. Res. Lett. 36, L23502.

van Herwijnen, A., Jamieson, B., 2005. High-speed photography of fractures in weak snowpack layers. Cold Reg. Sci. Technol. 43 (1–2), 71–82.

van Herwijnen, A., Schweizer, J., Heierli, J., 2010. Measurement of the deformation field associated with fracture propagation in weak snowpack layers. J. Geophys. Res. 115, F03042. doi:10.1029/2009JF001515.